BD-RIS-Enhanced Physical Layer Network Slicing for URLLC and eMBB Services

Diana Laura Fernández Duarte, Victoria Dala Pegorara Souto e Richard Demo Souza

***Abstract*— This paper investigates the use of Beyond-Diagonal Reconfigurable Intelligent Surfaces (BD-RIS) in 6G networks to support the coexistence of enhanced Mobile Broadband (eMBB) and Ultra-Reliable Low Latency Communications (URLLC) services, based on network slicing. Three BD-RIS architectures, Single-, Group-, and Fully-Connected, are evaluated under Heterogeneous Orthogonal Multiple Access (H-OMA) and Heterogeneous Non-Orthogonal Multiple Access (H-NOMA) schemes. The results show that the Group- and Fully-Connected architectures, when combined with optimal phase configuration, significantly expand the rate region and outperform conventional RIS.**

***Keywords*— eMBB, URLLC, Network Slicing, BD-RIS.**

I. Introduction

Sixth-generation (6G) networks are envisioned to support a wide range of heterogeneous services, including enhanced Mobile Broadband (eMBB), Ultra-Reliable Low Latency Communications (URLLC), and massive Machine-Type Communication (mMTC), each with distinct performance requirements: high data throughput (eMBB), ultra-low latency and high reliability (URLLC), and large-scale low-cost connectivity (mMTC) [1]. The simultaneous support of these services, especially in Industrial Internet of Things (IIoT) environments, presents substantial challenges [2]. To address these demands, network slicing has emerged as a promising approach by enabling the deployment of virtual, logically isolated network slices over a shared physical infrastructure [3]. However, traditional Orthogonal Multiple Access (OMA) schemes are inherently limited by the availability of orthogonal resources. In contrast, Non-Orthogonal Multiple Access (NOMA) offers a more flexible solution by allowing multiple users to share the same time-frequency resources through power-domain multiplexing, with interference managed via successive interference cancellation (SIC) at the receiver [4].

Several recent studies explore NOMA within network slicing. In [3], a theoretical comparison of Heterogeneous OMA (H-OMA) and Heterogeneous NOMA (H-NOMA) shows the advantage of H-NOMA under high service diversity. The study in [5] analyzes eMBB and URLLC coexistence in uplink scenarios, recommending NOMA when URLLC users have favorable channels. The work in [6] studies eMBB and mMTC coexistence, while [7] evaluates performance across H-OMA, H-NOMA, and RSMA schemes. In [8], H-NOMA is analyzed in a centralized RAN (C-RAN) with puncturing and SIC, revealing trade-offs between eMBB and URLLC. To optimize performance, [9] proposes a low-complexity algorithm for URLLC preemption in cluster-based NOMA-MIMO systems. Downlink power minimization using heuristic and feasible algorithms is addressed in [10]. Puncturing-based mechanisms [11], risk-aware transmission strategies [12], and resource allocation using max-matching diversity (MMD) [13] are also explored. Finally, a deep reinforcement learning (DRL)-based algorithm maintaining URLLC reliability while ensuring eMBB performance is proposed in [14].

Most of these works assume a direct link between users and the base station, which may be impractical in real-world scenarios [15]. Reconfigurable Intelligent Surfaces (RIS) offer a solution by introducing paths through passive reflective arrays [16]. Traditional RIS are modeled as diagonal impedance matrices, limiting beamforming to the incident side [16]. To overcome this, the Beyond Diagonal RIS (BD-RIS) architecture was proposed, enabling signal manipulation across the entire space via inter-element connectivity [17]. BD-RIS achieves comparable performance to conventional RIS with fewer elements, reducing cost and size [18].

Recent work has examined RIS-assisted service coexistence under H-OMA and H-NOMA. For instance, [15] shows performance gains for eMBB and URLLC using RIS. A two-stage algorithm in [19] optimizes eMBB data rates via resource block allocation and RIS phase matrix optimization. Additionally, [20] proposes joint power and phase optimization for NOMA-based eMBB/URLLC coexistence. These studies, however, are limited to single-connected RIS. The works in [21], [22] investigate BD-RIS under RSMA for URLLC broadcast channels, showing BD-RIS outperforms diagonal RIS in terms of max-min rate, although only single-service systems are considered.

Despite the potential of BD-RIS, its integration with network slicing remains largely unexplored. Moreover, the stringent latency constraints of URLLC hinder accurate channel state information (CSI) acquisition [3], complicating BD-RIS phase optimization. Additionally, H-NOMA introduces significant co-channel interference, making it an interference-limited scheme [23]. To bridge this gap, this work investigates BD-RIS-assisted slicing for URLLC and eMBB under H-OMA and H-NOMA. The main contributions are: i) BS-RIS enhances data rates for both URLLC and eMBB users

D. L. F. Duarte e V. D. P. Souto, National Institute of Telecommunications, Santa Rita do Sapucaí - MG, diana.duarte@mtel.inatel.br, victoria.souto@inatel.br; R. D. Souza, Federal University of Santa Catarina, Florianópolis - SC, richard.demo@ufsc.br; This work was funded by project XGM-AFCCT-2024-4-1-1, supported by xGMobile–EMBRAPII-Inatel Competence Center on 5G and 6G Networks, with resources from the PPI IoT/Manufacturing 4.0 program of MCTI grant number 052/2023, signed with EMBRAPII. This work has been partially funded by RNP, with resources from MCTIC, Grant No. 01245.020548/2021-07, under the Brazil 6G project of Inatel Radiocommunication Reference Center (Centro de Referência em Radiocomunicações - CRR), FAPEMIG (APQ-05305-23, APQ-04523-23, PPE-00124-23, RED-00194-23), and CNPq (305021/2021-4, 443974/2024-1).

even without CSI and under random phase configurations; ii) the proposed BD-RIS architectures outperform conventional single-connected RIS under optimal phase settings; iii) simulation results show that H-NOMA consistently outperforms H-OMA across the entire rate region.

II. System Model

This paper considers an uplink wireless system comprising a single-antenna base station (BS) assisted by a BD-RIS with $M = M_{\mathrm{h}} \times M_{\mathrm{v}}$ reflecting elements, where M_{h} and M_{v} are the numbers of horizontal and vertical elements, respectively. The network supports one URLLC user and K eMBB users, each equipped with a single antenna. We model the time-frequency resources as a grid with S time units, referred to as mini-slots, each carrying n_s symbols, and F frequency-domain resources. Due to the stringent latency requirements of URLLC, we assume that the BS lacks CSI for the URLLC user before transmission, as acquiring it would incur unacceptable signaling overhead. In contrast, the BS has prior CSI knowledge for eMBB users, whose traffic is more tolerant to latency. Accordingly, eMBB transmissions span a full time slot, while the URLLC transmission is confined to a mini-slot and a subset of frequency resources, $F_{\mathrm{u}} < F$, to meet its low-latency and high-reliability constraints.

A. BD-RIS Architecture

We analyze the integration of BD-RIS within this network slicing context by considering various interconnection architectures, which define how the RIS elements are linked via a reconfigurable impedance network [17]:

- **Single-Connected BD-RIS:** Also known as classical RIS, this architecture has no inter-element connections. Each element is independently grounded through a reconfigurable impedance. The scattering matrix is diagonal: $\mathbf{\Phi} = \mathrm{diag}\left(e^{j\theta_1}, \ldots, e^{j\theta_M}\right)$,where θ_m denotes the phase shift of the m-th element [17].
- **Fully-Connected BD-RIS:** The M ports are interconnected via reconfigurable impedance elements, enabling complex signal transformations. The scattering matrix $\mathbf{\Phi}$ is symmetric unitary, $\mathbf{\Phi} = \mathbf{\Phi}^T, \quad \mathbf{\Phi}\mathbf{\Phi}^H = \mathbf{I}_M$ [17].
- **Group-Connected BD-RIS:** The M ports are divided into N_{G} groups of $M_{\mathrm{G}} = M/N_{\mathrm{G}}$ elements; only elements within a group are interconnected. The scattering matrix is block diagonal $\mathbf{\Phi} = \mathrm{blockdiag}(\mathbf{\Phi}_1, \ldots, \mathbf{\Phi}_{N_{\mathrm{G}}})$, with each block satisfying $\mathbf{\Phi}_g = \mathbf{\Phi}_g^T$ and $\mathbf{\Phi}_g\mathbf{\Phi}_g^H = \mathbf{I}_{M_{\mathrm{G}}}$ [17]. This model generalizes both the single-connected case ($M_{\mathrm{G}} = 1$) and the fully connected case ($M_{\mathrm{G}} = M$).

In this paper, three different deployment scenarios are considered for evaluation, as described next.

B. *Scenario 1: URLLC assisted by BD-RIS*

In Scenario 1, Fig. 1(a), the BD-RIS supports only the URLLC user, while the K eMBB users communicate directly with the BS. The received signal $y_{s,f}$ for the s-th minislot, $s \in 1, ..., S$, and the f-th frequency, $f \in 1, ..., F$, is

$$y_{s,f} = \sqrt{\beta_{\mathrm{b},f}} h_{\text{BS-b},f} \mathbf{x}_{\mathrm{b},s,f} + \sqrt{\beta_u} h_{\mathrm{u},f} \mathbf{x}_{\mathrm{u},s,f} + \mathbf{z}_{s,f}, \quad (1)$$

where the subscripts u and b indicate the eMBB user and the URLLC user, respectively. The signal transmitted by user $i \in$ b,u is represented by $\mathbf{x}_{i,s,f} \in \mathbb{C}^{1\times n_s}$, while $\mathbf{z}_{s,f} \in \mathbb{C}^{1\times n_s}$ is the additive white Gaussian noise with zero mean and unit variance. The direct channel between the BS and the k-th eMBB user is denoted as $h_{\text{BS-b},f} \in \mathbb{C}^{1\times 1}$, whereas $h_{\mathrm{u},f}$ represents the combined channel from the BS to the URLLC user, which includes both the direct and the reflected paths through the BD-RIS. This combined channel is expressed as

$$h_{\mathrm{u},f} = \mathbf{h}_{\text{BS-BDRIS},f} \mathbf{\Phi} \mathbf{h}^{\mathrm{H}}_{\text{BDRIS-u},f} + h^{\mathrm{H}}_{\text{BS-u},f}, \quad (2)$$

where $\mathbf{h}$BS-BDRIS, $f \in \mathbb{C}^{1\times M}$ is the channel between the BS and the BD-RIS, while $\mathbf{h}$BDRIS-u, $f \in \mathbb{C}^{M\times 1}$ represents the channel between the BD-RIS and the URLLC user. Additionally, $h_{\text{BS-u},f} \in \mathbb{C}^{1\times 1}$ is the direct channel between the BS and the URLLC user. The BD-RIS scattering matrix is $\mathbf{\Phi}$, and its specific model depends on the impedance network topology.

Moreover, we assume the fading follows a Rician distribution. Therefore, the channel $h_{\mathrm{BS}-i}$ for $i \in$ b,u and the channel $\mathbf{h}_{\mathrm{BDRIS}-j}$ for $j \in$ BS, u are expressed as

$$h_{\mathrm{BS}-i} = \sqrt{\frac{\kappa}{1+\kappa}} h^{\mathrm{LoS}}_{\mathrm{BS}-i} + \sqrt{\frac{1}{1+\kappa}} h^{\mathrm{nLoS}}_{\mathrm{BS}-i}, \quad (3)$$

$$\mathbf{h}_{\mathrm{BDRIS}-j} = \sqrt{\frac{\kappa}{1+\kappa}} \mathbf{h}^{\mathrm{LoS}}_{\mathrm{BDRIS}-j} + \sqrt{\frac{1}{1+\kappa}} \mathbf{h}^{\mathrm{nLoS}}_{\mathrm{BDRIS}-j}, \quad (4)$$

where $h^{\mathrm{LoS}}_{\mathrm{BS}-i}$ and $\mathbf{h}\mathrm{BDRIS} - j^{\mathrm{LoS}}$ are the deterministic LoS components of the channels. The non-LoS (NLoS) components are $h\mathrm{BS} - i^{\mathrm{nLoS}}$ and $\mathbf{h}^{\mathrm{nLoS}}_{\mathrm{BDRIS}-j}$, modeled as complex Gaussian random variables with zero mean and unit variance. The Rician factor, κ, is the ratio between the power of the LoS and the NLoS components.

Additionally, β_{u} and $\beta_{\mathrm{b},f}$ are the path loss between the BS and the URLLC user (via BD-RIS), and between the BS and the eMBB users, respectively. Each eMBB user transmits on a distinct frequency channel, and that $\beta_{\mathrm{b},f}$ is constant across all frequencies. Therefore, β_{b} and β_{u} are given by [24]

$$\beta_{\mathrm{b}} = G_{\mathrm{t}} + G_{\mathrm{r}} - 10\log_{10}(d_{\text{BS-b}}) - \beta_0, \quad (5)$$

$$\beta_{\mathrm{u}} = G_{\mathrm{t}} + G_{\mathrm{r}} - 10\log_{10}(D) - \beta_1, \quad (6)$$

where G_{t} and G_{r} denote the gains of the transmit and receive antennas, α is the path loss exponent, $d_{\text{BS-b}}$ is the distance between the BS and the k-th eMBB user, β_0 and β_1 are constants. Additionally, $D = \left(ab\cos(\phi_{\mathrm{c}})/d_{\text{BS-BDRIS}}d_{\text{BDRIS-u}}\right)^2$, where $a = M_{\mathrm{h}}d_{\mathrm{BDRIS}}\lambda$ and $b = M_{\mathrm{v}}d_{\mathrm{BDRIS}}\lambda$ are the parameters representing the dimensions of the BD-RIS, depending on the number of horizontal elements M_{h} and vertical elements M_{v}, the distance d_{BDRIS} that separates these elements, and the wavelength λ. In addition, $d_{\text{BS-BDRIS}}$ and $d_{\text{BDRIS-u}}$ denote the distances between the BS and the BD-RIS, and between the BD-RIS and the URLLC user, respectively. Finally, the angle of arrival at the BD-RIS is $\phi_{\mathrm{c}} = \arctan(y_0/x_0)$, where (x_0, y_0) is the position of the BD-RIS.

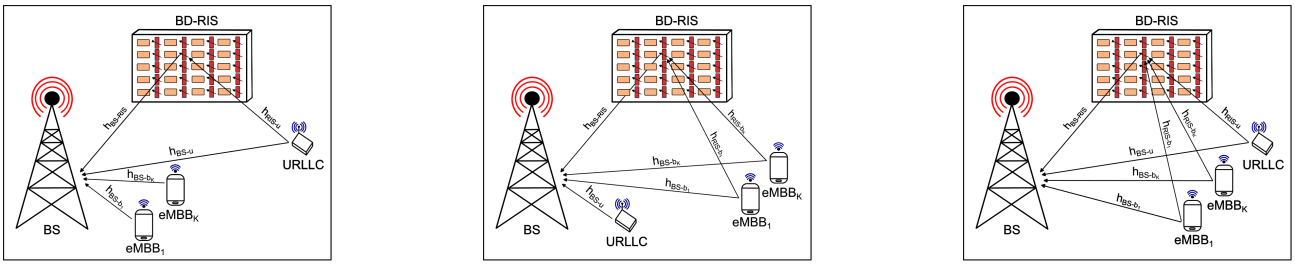

(a) Scenario 1 (b) Scenario 2 (c) Scenario 3

Fig. 1: Evaluated scenarios. (a) *Scenario 1*: The BD-RIS assists only the URLLC user; (b) *Scenario 2*: The BD-RIS assists only the eMBB users; (c) *Scenario 3*: The BD-RIS assists both URLLC and eMBB users.

C. *Scenario 2: eMBB assisted by BD-RIS:*

In Scenario 2, Fig. 1(b), the URLLC user communicates directly with the BS, while the K eMBB users communicate with the BS with the assistance of the BD-RIS. This configuration requires a reformulation of the received signal $y_{s,f}$ at the BS. Therefore, $y_{s,f}$ for the s-th minislot, $s \in 1, ..., S$, and the f-th frequency, $f \in 1, ..., F$, is expressed as

$$y_{s,f} = \sqrt{\beta_{\mathrm{b},f}} h_{\mathrm{b},f} \mathbf{x}_{\mathrm{b},s,f} + \sqrt{\beta_u} h_{\text{ BS-u},f} \mathbf{x}_{\mathrm{u},s,f} + \mathbf{z}_{s,f}, \quad (7)$$

where $h_{\text{BS-u},f} \in \mathbb{C}^{1\times 1}$ is the direct channel between the BS and the URLLC user, and $h_{\mathrm{b},f}$ is the composite channel between the BS and the k-th eMBB user, comprising both the direct and the cascaded path via the BD-RIS. The channel $h_{\mathrm{b},f}$ is

$$h_{\mathrm{b},f} = \mathbf{h}_{\text{BS-BDRIS},f} \mathbf{\Phi} \mathbf{h}^{\mathrm{H}}_{\text{BDRIS-b},f} + h^{\mathrm{H}}_{\text{BS-b},f}, \quad (8)$$

where $\mathbf{h}_{\text{BS-BDRIS},f} \in \mathbb{C}^{1\times M}$ is the channel between the BS and the BD-RIS, $\mathbf{h}_{\text{BDRIS-b},f} \in \mathbb{C}^{M\times 1}$ is the channel vector from the BD-RIS to the k-th eMBB user, and $h_{\text{BS-b},f} \in \mathbb{C}^{1\times 1}$ is the direct channel between the BS and the k-th eMBB user. The channel $h_{\text{BS}-i}$ for $i \in \{\mathrm{b},\mathrm{u}\}$ is based on (3), while $\mathbf{h}_{\text{BDRIS}-j}$ for $j \in \{\text{BS, b}\}$ is given by (4). Since the path loss components depend if the link is direct with the BS or via BD-RIS, β_{u} is computed based on (5) considering the distance between the BS and the URLLC user ($d_{\text{BS-u}}$). Similarly, β_{b} is computed by (6) considering the distance between the BD-RIS and the eMBB user ($d_{\text{BDRIS-b}}$).

D. *Scenario 3: URLLC and eMBB assisted by BD-RIS*

In the third scenario, Fig. 1(c), both the URLLC and the K eMBB users are assisted by the BD-RIS. The received signal $y_{s,f}$, $s \in \{1, \ldots, S\}$ and $f \in \{1, \ldots, F\}$, is

$$y_{s,f} = \sqrt{\beta_{\mathrm{b},f}} h_{\mathrm{b},f} \mathbf{x}_{\mathrm{b},s,f} + \sqrt{\beta_u} h_{\mathrm{u},f} \mathbf{x}_{\mathrm{u},s,f} + \mathbf{z}_{s,f}, \quad (9)$$

where $h_{\mathrm{b},f}$ and $h_{\mathrm{u},f}$ are given by (8) and (2), respectively. The direct channel between the BS and user $i \in \{\mathrm{b},\mathrm{u}\}$, denoted by $h_{\text{BS}-i,f}$, is defined as (3), while the channel between the BD-RIS and node $i \in \{\text{BS}, \mathrm{b}, \mathrm{u}\}$ ($h_{\text{BDRIS}-i,f}$) is given by (4). Since all users are assisted by the BD-RIS, the path loss components β_{u} and β_{b} are computed based on (6); for β_{b}, the distance $d_{\text{BDRIS-u}}$ is replaced by $d_{\text{BDRIS-b}}$.

III. Metrics and Beamforming Design

A. *Performance Metrics: Achievable Rate*

To assess system performance under the coexistence of eMBB and URLLC services enabled by physical-layer network slicing with H-OMA or H-NOMA, a scenario with one URLLC user and K eMBB users is considered. Each eMBB user is preassigned a frequency resource by the BS, and URLLC decoding is prioritized due to its low-latency needs. Performance is evaluated via the achievable rate pair $(r_{\text{sum,b}},\ r_{\mathrm{u}})$ under reliability constraints $(\epsilon_{\mathrm{b}},\ \epsilon_{\mathrm{u}})$, with user channel gains defined as $\Gamma_{i,f} = \beta_i |h_{i,f}|^2$, where $i \in \mathrm{b}, \mathrm{u}$.

1) H-OMA: In H-OMA, F_{u} frequency channels are dedicated exclusively to URLLC traffic, while the remaining $F_{\mathrm{b}} = F - F_{\mathrm{u}}$ channels serve only $K = F_{\mathrm{b}}$ eMBB users. The outage probability of the URLLC user is given by [3]

$$P_{\mathrm{u}}^{\text{H-OMA}} = \Pr\left(\frac{1}{F_{\mathrm{u}}} \sum_{f=1}^{F_{\mathrm{u}}} \log_2(1 + \Gamma_{\mathrm{u},f}) < r_{\mathrm{u}}^{\text{H-OMA}} \right), \quad (10)$$

where $r_{\mathrm{u}}^{\text{H-OMA}}$ is the achievable rate for the URLLC user. Moreover, the total achievable rate for the eMBB service is [3]

$$r_{\text{sum,b}} = \sum_{f=1}^{F_{\mathrm{b}}} r_{\mathrm{b},f} = \sum_{f=1}^{F_{\mathrm{b}}} \log_2(1 + \Gamma_{\mathrm{b},f}). \quad (11)$$

2) H-NOMA: In H-NOMA, all F frequency channels are simultaneously shared between both service types, implying $F_{\mathrm{u}} = F_{\mathrm{b}} = F$. We assume $K = F_{\mathrm{b}}$ eMBB users, each occupying a unique frequency resource f, with the BS assigning channels in a scheduling step preceding data transmission. Therefore, the outage probability of the URLLC user is [3]

$$P_{\mathrm{u}}^{\text{H-NOMA}} = \Pr\left(\frac{1}{F} \sum_{f=1}^{F} \log_2\left(1 + \frac{\Gamma_{\mathrm{u},f}}{\Gamma_{\mathrm{b},f}}\right) < r_{\mathrm{u}}^{\text{H-NOMA}} \right) \quad (12)$$

where $r_{\mathrm{u}}^{\text{H-NOMA}}$ is the achievable rate for the URLLC user. The total achievable rate for the eMBB service is (11). From (12), URLLC performance under H-NOMA is sensitive to interference, particularly from the channel gains of co-scheduled eMBB users. This makes user clustering a critical factor in system performance [25]. Thus, we consider clusters with $K = F_{\mathrm{b}}$ eMBB users and one URLLC user.

B. BD-RIS Beamforming Design

An effective beamforming strategy using BD-RIS seeks to optimize performance by adjusting phase shifts, contingent on CSI availability at the BS. The beamforming design for each scenario in Fig. 1 is as follows.

- **Scenario 1 (Fig. 1a):** Without CSI at the URLLC user, the BD-RIS employs a random phase configuration. Despite being suboptimal, prior work shows that random settings in single-connected RIS yield performance gains [26]. We extend this approach to group and fully connected architectures.
- **Scenario 2 (Fig. 1b):** With BD-RIS assisting only eMBB users and CSI available at the BS, the scattering matrix $\mathbf{\Phi}$ is optimally configured for constructive alignment. For the single-connected case, the optimal phase shifts are

$$\theta^* = \arg(\mathbf{h}_{\text{BS-b}}) - \arg(\mathbf{h}_{\text{BS-BDRIS}}) - \arg(\mathbf{h}_{\text{BDRIS-b}}) \quad (13)$$

  For the group and fully connected cases, optimal design for $\mathbf{\Phi}$ is adopted from [27], assuming multiple users.
- **Scenario 3 (Fig. 1c):** Phase shifts for URLLC are random due to unavailable CSI, while for eMBB users they are optimized as in Scenario 2.

IV. Numerical Results

We consider a simulation setup where $(x_0,\ y_0)$, $(x_\text{i},\ y_\text{i})$, $(x_\text{u},\ y_\text{u})$, and $(x_\text{b},\ y_\text{b})$ represent the positions of the BS, the BD-RIS, the URLLC user, and the eMBB users, respectively. For simplicity, it is assumed that the K eMBB users are located approximately at the same distance from the BS, at $(x_\text{b},\ y_\text{b})$. For all scenarios, we assume $(x_0,\ y_0) = (80,\ 2)$ m and $(x_\text{i},\ y_\text{i}) = (0,\ 2)$ m, while the user positions vary. Moreover, the simulation parameters are set as follows: $f_\text{c} = 4$ GHz, $d_\text{RIS} = 0.5$, $G_\text{t} = G_\text{r} = 3$ dBi, $\alpha = 2.2$, $\beta_0 = 41.98$ dB, and $\beta_1 = 21.98$ dB. In addition, we fix $M_\text{h} = 5$ and vary M_v, such that $M \in \{20,\ 40\}$. Finally, we define the reliability thresholds as $\epsilon_\text{u} = 10^{-5}$ and $\epsilon_\text{b} = 10^{-3}$. The results were obtained using MATLAB®, averaging over a total of 10^7 independent channel realizations.

Scenario 1 (Fig. 1(a)): The BD-RIS assists only the URLLC user, whose phase shifts are configured randomly to avoid latency. Despite the non-optimized configuration, Fig. 2 shows that increasing the number of RIS elements from $M = 20$ to $M = 40$ improves the URLLC rate. Under H-NOMA, the URLLC rate r_u increases from approximately 0.26 bps/Hz (no RIS) to 0.34 bps/Hz with $M = 40$ at an eMBB sum rate of 7.25 bps/Hz. Additionally, the eMBB rate at $r_\text{u} \approx 0.35$ bps/Hz improves by about 4.5 bps/Hz with RIS deployment. H-NOMA consistently outperforms H-OMA.

Scenario 2 (Fig. 1(b)): The RIS supports only the eMBB users, with available CSI enabling optimal phase alignment. Fig. 3 shows that the eMBB sum rate reaches 17.1 bps/Hz with a conventional RIS of 40 elements, compared to 2.7 bps/Hz without RIS. A fully-connected architecture further improves performance under H-NOMA by about 3.7 bps/Hz over the single-connected case. The group-connected configuration with $N_\text{G} = 10$ achieves around 20.1 bps/Hz, only 3.5% lower

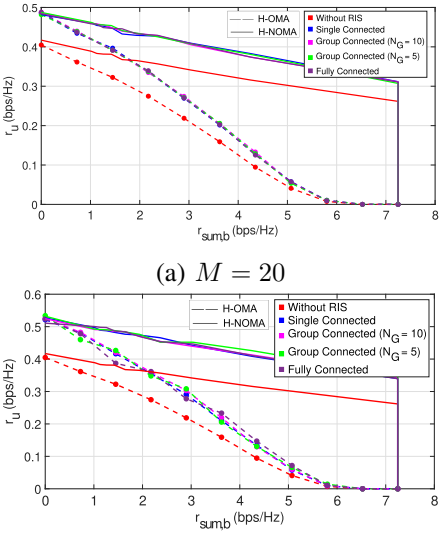

(a) $M = 20$

(b) $M = 40$

Fig. 2: Rate region for Scenario in Fig. 1a considering $N \in \{20, 40\}$, $(x_\text{u} = 10, y_\text{u} = 0)$ m, and $(x_\text{b} = 40, y_\text{b} = 0)$ m.

than the fully-connected case, providing a good complexity-performance trade-off. H-NOMA again outperforms H-OMA across the region.

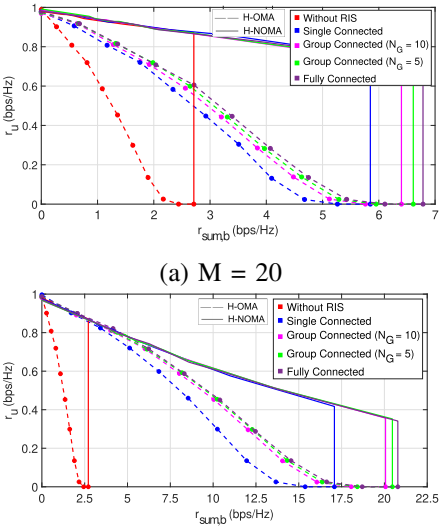

(a) M = 20

(b) M = 40

Fig. 3: Rate region for Scenario in Fig. 1b considering $N \in \{20, 40\}$, $(x_\text{u} = 40, y_\text{u} = 0)$ m, and $(x_\text{b} = 10, y_\text{b} = 0)$ m.

Scenario 3 (Fig. 1(c)): The BD-RIS supports both user types. While the URLLC user adopts random phase shifts, the eMBB users benefit from optimized configuration. Fig. 4 shows that a conventional RIS with $M = 40$ increases the eMBB sum rate from 3.1 bps/Hz (no RIS) to 12.7 bps/Hz. The URLLC rate sees a smaller gain of about 0.1 bps/Hz. A fully-connected configuration achieves up to 12.73 bps/Hz (a 2.7 bps/Hz improvement), and a group-connected design with $N_\text{G} = 10$ attains approximately 14.9 bps/Hz. Again, H-NOMA proves superior to H-OMA in all cases.

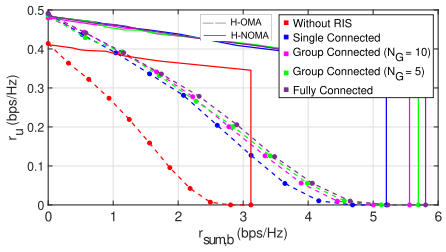

(a) M = 20

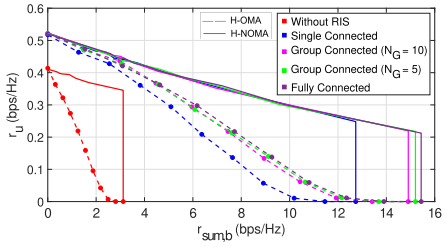

(b) M = 40

Fig. 4: Rate region for Scenario in Fig. 1c considering $N \in \{20, 40\}$, $(x_{\mathrm{u}} = 10, y_{\mathrm{u}} = 0)$ m and $(x_{\mathrm{b}} = 15, y_{\mathrm{b}} = 0)$ m.

V. Conclusion

This study investigates the integration of a BD-RIS to concurrently support uplink transmissions of both eMBB and URLLC services to a common BS. The analysis focuses on the achievable rate region under the reliability constraints of both service types, considering two multiple access schemes: H-OMA and H-NOMA. The results demonstrate that incorporating a BD-RIS, even with randomly configured phase shifts, leads to noticeable performance gains. These gains are further amplified when employing group-connected or fully connected architectures, coupled with optimal phase design under the assumption of perfect CSI at the BS. Moreover, the findings consistently show that H-NOMA outperforms H-OMA across all evaluated BD-RIS configurations and scenarios.

Referências

[1] H. Tullberg, P. Popovski, Z. Li, M. A. Uusitalo, A. Hoglund, O. Bulakci, M. Fallgren, and J. F. Monserrat, "The METIS 5G System Concept: Meeting the 5G Requirements," *IEEE Communications Magazine*, vol. 54, no. 12, pp. 132–139, 2016.

[2] B. S. Khan, S. Jangsher, A. Ahmed, and A. Al-Dweik, "URLLC and eMBB in 5G Industrial IoT: A Survey," *IEEE Open Journal of the Communications Society*, vol. 3, pp. 1134–1163, 2022.

[3] P. Popovski, K. F. Trillingsgaard, O. Simeone, and G. Durisi, "5G Wireless Network Slicing for eMBB, URLLC, and mMTC: A Communication-Theoretic View," *IEEE Access*, vol. 6, pp. 55 765–55 779, 2018.

[4] E. N. Tominaga, H. Alves, O. L. A. López, R. D. Souza, J. L. Rebelatto, and M. Latva-aho, "Network Slicing for eMBB and mMTC with NOMA and Space Diversity Reception," in *2021 IEEE 93rd Vehicular Technology Conference (VTC2021-Spring)*, 2021, pp. 1–6.

[5] E. N. Tominaga, H. Alves, R. D. Souza, J. Luiz Rebelatto, and M. Latva-aho, "Non-Orthogonal Multiple Access and Network Slicing: Scalable Coexistence of eMBB and URLLC," in *2021 IEEE 93rd Vehicular Technology Conference (VTC2021-Spring)*, 2021, pp. 1–6.

[6] E. N. Tominaga, H. Alves, O. L. A. López, R. D. Souza, J. L. Rebelatto, and M. Latva-aho, "Network Slicing for eMBB and mMTC with NOMA and Space Diversity Reception," in *2021 IEEE 93rd Vehicular Technology Conference (VTC2021-Spring)*, 2021, pp. 1–6.

[7] Y. Liu, B. Clerckx, and P. Popovski, "Network Slicing for eMBB, URLLC, and mMTC: An Uplink Rate-Splitting Multiple Access Approach," *IEEE Transactions on Wireless Communications*, vol. 23, no. 3, pp. 2140–2152, 2024.

[8] R. Kassab, O. Simeone, and P. Popovski, "Coexistence of URLLC and eMBB Services in the C-RAN Uplink: An Information-Theoretic Study," in *2018 IEEE Global Communications Conference (GLOBECOM)*, 2018, pp. 1–6.

[9] Q. Chen, J. Wang, and H. Jiang, "URLLC and eMBB Coexistence in MIMO Non-orthogonal Multiple Access Systems," 2021. [Online]. Available: https://arxiv.org/abs/2109.05725

[10] F. Saggese, M. Moretti, and P. Popovski, "Power Minimization of Downlink Spectrum Slicing for eMBB and URLLC Users," *IEEE Transactions on Wireless Communications*, vol. 21, no. 12, pp. 11 051–11 065, 2022.

[11] A. K. Bairagi, M. S. Munir, M. Alsenwi, N. H. Tran, S. S. Alshamrani, M. Masud, Z. Han, and C. S. Hong, "Coexistence Mechanism Between eMBB and uRLLC in 5G Wireless Networks," *IEEE Transactions on Communications*, vol. 69, no. 3, pp. 1736–1749, 2021.

[12] M. Alsenwi, N. H. Tran, M. Bennis, A. Kumar Bairagi, and C. S. Hong, "eMBB-URLLC Resource Slicing: A Risk-Sensitive Approach," *IEEE Communications Letters*, vol. 23, no. 4, pp. 740–743, 2019.

[13] E. J. dos Santos, R. D. Souza, J. L. Rebelatto, and H. Alves, "Network Slicing for URLLC and eMBB With Max-Matching Diversity Channel Allocation," *IEEE Communications Letters*, vol. 24, no. 3, pp. 658–661, 2020.

[14] M. Alsenwi, N. H. Tran, M. Bennis, S. R. Pandey, A. K. Bairagi, and C. S. Hong, "Intelligent Resource Slicing for eMBB and URLLC Coexistence in 5G and Beyond: A Deep Reinforcement Learning Based Approach," *IEEE Transactions on Wireless Communications*, vol. 20, no. 7, pp. 4585–4600, 2021.

[15] V. D. P. Souto, S. Montejo-Sánchez, J. L. Rebelatto, R. D. Souza, and B. F. Uchôa-Filho, "IRS-Aided Physical Layer Network Slicing for URLLC and eMBB," *IEEE Access*, vol. 9, pp. 163 086–163 098, 2021.

[16] H. Li, S. Shen, and B. Clerckx, "Beyond Diagonal Reconfigurable Intelligent Surfaces: From Transmitting and Reflecting Modes to Single-, Group-, and Fully-Connected Architectures," *IEEE Transactions on Wireless Communications*, vol. 22, no. 4, pp. 2311–2324, 2023.

[17] S. Shen, B. Clerckx, and R. Murch, "Modeling and Architecture Design of Reconfigurable Intelligent Surfaces Using Scattering Parameter Network Analysis," *IEEE Transactions on Wireless Communications*, vol. 21, no. 2, pp. 1229–1243, 2022.

[18] H. Li, S. Shen, and B. Clerckx, "Beyond Diagonal Reconfigurable Intelligent Surfaces: A Multi-Sector Mode Enabling Highly Directional Full-Space Wireless Coverage," *IEEE Journal on Selected Areas in Communications*, vol. 41, no. 8, pp. 2446–2460, 2023.

[19] X. Shen, Z. Zeng, and X. Liu, "RIS-Assisted Network Slicing Resource Optimization Algorithm for Coexistence of eMBB and URLLC," *Electronics*, vol. 11, no. 16, 2022. [Online]. Available: https://www.mdpi.com/2079-9292/11/16/2575

[20] J. Na, J. Kang, and J. Kang, "Intelligent Reflecting Surface-Assisted Uplink NOMA for eMBB and URLLC Coexistence," *IEEE Transactions on Vehicular Technology*, vol. 73, no. 5, pp. 7406–7411, 2024.

[21] M. Soleymani, I. Santamaria, E. A. Jorswieck, and B. Clerckx, "Optimization of Rate-Splitting Multiple Access in Beyond Diagonal RIS-Assisted URLLC Systems," *IEEE Transactions on Wireless Communications*, vol. 23, no. 5, pp. 5063–5078, 2024.

[22] M. Soleymani, A. Zappone, E. Jorswieck, M. Di Renzo, and I. Santamaria, "Rate Region of RIS-Aided URLLC Broadcast Channels: Diagonal Versus Beyond Diagonal Globally Passive RIS," *IEEE Wireless Communications Letters*, vol. 14, no. 2, pp. 320–324, 2025.

[23] L. Dai, B. Wang, Z. Ding, Z. Wang, S. Chen, and L. Hanzo, "A survey of non-orthogonal multiple access for 5g," *IEEE Communications Surveys Tutorials*, vol. 20, no. 3, pp. 2294–2323, 2018.

[24] "Further advancements for E-UTRA physical layer aspects (release 9)," 3GPP, Tech. Rep., Mar 2010.

[25] Z. Ding, P. Fan, and H. V. Poor, "Impact of user pairing on 5g nonorthogonal multiple-access downlink transmissions," *IEEE Transactions on Vehicular Technology*, vol. 65, no. 8, pp. 6010–6023, 2016.

[26] Q. Tao, S. Zhang, C. Zhong, and R. Zhang, "Intelligent Reflecting Surface Aided Multicasting With Random Passive Beamforming," *IEEE Wireless Communications Letters*, vol. 10, no. 1, pp. 92–96, 2021.

[27] M. Nerini, S. Shen, and B. Clerckx, "Closed-Form Global Optimization of Beyond Diagonal Reconfigurable Intelligent Surfaces," *IEEE Transactions on Wireless Communications*, vol. 23, no. 2, pp. 1037–1051, 2024.